Journal of Fluids and Structures (1999) **13,** 251–268
Article No.: jfls.1998.0197 available online at http://www.idealibrary.com. on IDEAL

VIBRATION AND STABILITY ANALYSIS OF CANTILEVERED TWO-PIPE SYSTEMS CONVEYING DIFFERENT FLUIDS

M. A. LANGTHJEM† AND Y. SUGIYAMA

Department of Aerospace Engineering, Osaka Prefecture University, 1-1 Gakuen-cho, Sakai-shi, Osaka 599-8531, Japan

(Received 21 April 1998 and in revised form 19 October 1998)

This paper considers the dynamic stability of plane transverse oscillations of two cantilevered pipes interconnected along their outer radii and conveying different fluids with different flow speeds. Stability curves depicting the relation between the two flow speeds at the stability boundary are shown for a number of fluid-structure mass ratios. One fluid flow may dissipate energy delivered to the system by the other, if the speed of the first one is not too large. One pipe can thus be thought of as a stabilizer to the other, with the aim of increasing the critical speed of the primary flow. The stabilizing effect of one fluid on the other is clarified through considerations of an energy equation together with flutter oscillation shapes. The energy equation is also used to derive a relation between the two flow speeds and the phase speed of the flow-induced travelling bending wave.

1. INTRODUCTION

DYNAMIC STABILITY of cantilevered fluid-conveying pipes has formed the subject of a large number of papers since the early 1960s. The transfer of energy between the flowing fluid and the pipe was discussed by Benjamin (1961), thus explaining the mechanism behind the flow-induced unstable oscillations ("flutter") that occur when the flow rate exceeds a critical value. The effect of system parameters (e.g., mass ratio, pipe dimensions, damping, gravity) has been studied extensively, and recently nonlinear dynamic aspects have been studied intensively. Reviews were published by Païdoussis & Issid (1974), by Païdoussis (1987) and by Païdoussis & Li (1993). Interest in the fluid-conveying pipe problem has been driven partly by the fact that the basic fluid-structure coupling is similar to a variety of "flutter problems", including flapping flags and sails (Lamb 1932; Taneda 1968), aircraft wings (Dowell *et al.* 1989) and human snoring (Huang 1995). The problem of flutter induced by a pure rocket thrust, which has applications to missiles, spacecraft and space structure, is also closely related (Sugiyama *et al.* 1995a, b).

Most studies are concerned with a single cantilever conveying a single fluid. An exception is a paper by Hannoyer & Païdoussis (1978) on the combined effects of simultaneous internal and external axial flows, which brings forth many interesting aspects of two interacting fluid loadings and concludes that "the state of the system with both internal and external flows present cannot in general be inferred from knowledge of its state when subjected separately to the internal and the external flow." It was shown that if the flutter

† Present address: Vibration and Noise Control Laboratory, Takasago R&D Center, Mitsubishi Heavy Industries, Ltd., 2-1-1 Shinhama, Arai-cho, Takasago, Hyogo Prefecture, 676 Japan.

0889–9746/99/020251 + 18 $30.00

boundary has been passed due to the action of a single fluid flow, the system can be restabilized by increasing the flow rate of the other fluid. Païdoussis & Besançon (1980) generalized the analysis to an array of cylinders; however, they considered simply supported pipes where divergence is the only possible type of instability. Examples of applications include axial heat exchangers and stream generators.

The object of the present paper is to further clarify the effects of two interacting axial fluid flows on the dynamic stability of a cantilevered pipe system. Due to the great complexity of the external flow model, Hannoyer & Païdoussis (1978) could not present an extensive parameter study. However, their results were compared with experiments and reasonable good agreement was found. The present paper considers a system of two cantilevered pipes, interconnected along their outer radii and thus, interaction between two internal flows. Applications may be found in the offshore industry, for example in connection with drilling for oil.

The description of an internal flow is considerably simpler than an external flow. The fundamental coupling between the structure and axial flow is similar. However, in the case of external flow it is modified by boundary layer effects. [Hannoyer & Païdoussis (1978) show how this may be taken into account.] Furthermore, the dynamics is altered by axial and lateral viscous forces. Thus, a cantilever subjected to external axial flow loses stability by divergence. At a higher flow speed flutter is observed. To focus on the inviscid fluid loading, the simplest configuration is considered in this paper. The effects of damping and gravity are thus not taken into account.

The paper is divided into seven sections. Section 2 describes the analysis of plane transverse oscillations. As the cross-section is not axisymmetric, the fluid loading may induce torsional instability. Section 3 addresses this problem, applying the equations derived by Hermann & Nemat–Nasser (1967) for a two-pipe system having a cross-section with two axes of symmetry. For three specific examples, it is found that transverse flutter occurs at much lower flow speeds than torsional instability. In light of this, only transverse oscillations are considered in the remainder of the paper.

Section 4 presents stability diagrams, depicting the relation between the two flow speeds at the flutter limit for a number of different fluid–structure mass ratio parameters. The case of simultaneous "forward" and "reverse" flow in a system of two identical pipes conveying identical fluids is also discussed, however noting that the application of the same boundary conditions to forward and reverse flow may be questioned [see Païdoussis (1997) for a discussion]. Within the framework of the present theory, the pipe with forward flow provides a very effective means of stabilization of the aspirating pipe as the forward flow cancels out the negative fluid damping induced by the reverse flow. The resulting fluid loading is thus a pure "follower" load, as by Beck's column [see, e.g., Bolotin (1963)]. Examples of aspirating pipes include deep-water risers for ocean mining (Païdoussis & Luu 1992) and the 'Deep Ocean Water Upwelling Machine' for increasing the primary production in the sea and creating new fishing grounds (Ouchi & Nakahara 1998).

In Section 5, the equation for energy balance at the flutter limit of Benjamin (1961) is applied in the deviation of a relation between the two flow speeds and the phase speed of the flow-induced travelling bending wave. It is found that, at the flutter limit, the phase speed at the end of the pipe system equals the ratio (total momentum flux)/(total mass flow rate). For a single pipe, this ratio reduces to the (single) flow speed, in agreement with the result for a free axisymmetric jet of Batchelor & Gill (1962).

In Section 6, the physical understanding of the stabilizing effect one fluid may have on the other is clarified by considering Benjamin's energy equation together with flutter oscillation shapes. Finally, the main conclusions are summarized in Section 7.

2. EQUATION OF MOTION FOR TRANSVERSE OSCILLATIONS

The system is sketched in Figure 1. The undisturbed flow of incompressible fluid through the pipes is in the direction of the axis x, entering at $x = 0$. Transverse deflections occur in the vertical plane in the direction of the axis y. One pipe, to be referred to as pipe A, has specific mass m_A and bending stiffness EI_A. The fluid flowing through it has specific mass M_A. For the other one, pipe B, the corresponding quantities are m_B, EI_B and M_B. Structural (internal) and aerodynamic (external) damping is ignored. For this system, Benjamin (1961) showed that Hamilton's principle can be written as

$$\delta \int_{t_1}^{t_2} (L + W_C)\,\mathrm{d}t + \int_{t_1}^{t_2} \delta W_N \,\mathrm{d}t = 0, \tag{1}$$

where

$$L = T_{\text{pipes}} + T_{\text{fluid}} - V_{\text{pipes}}. \tag{2}$$

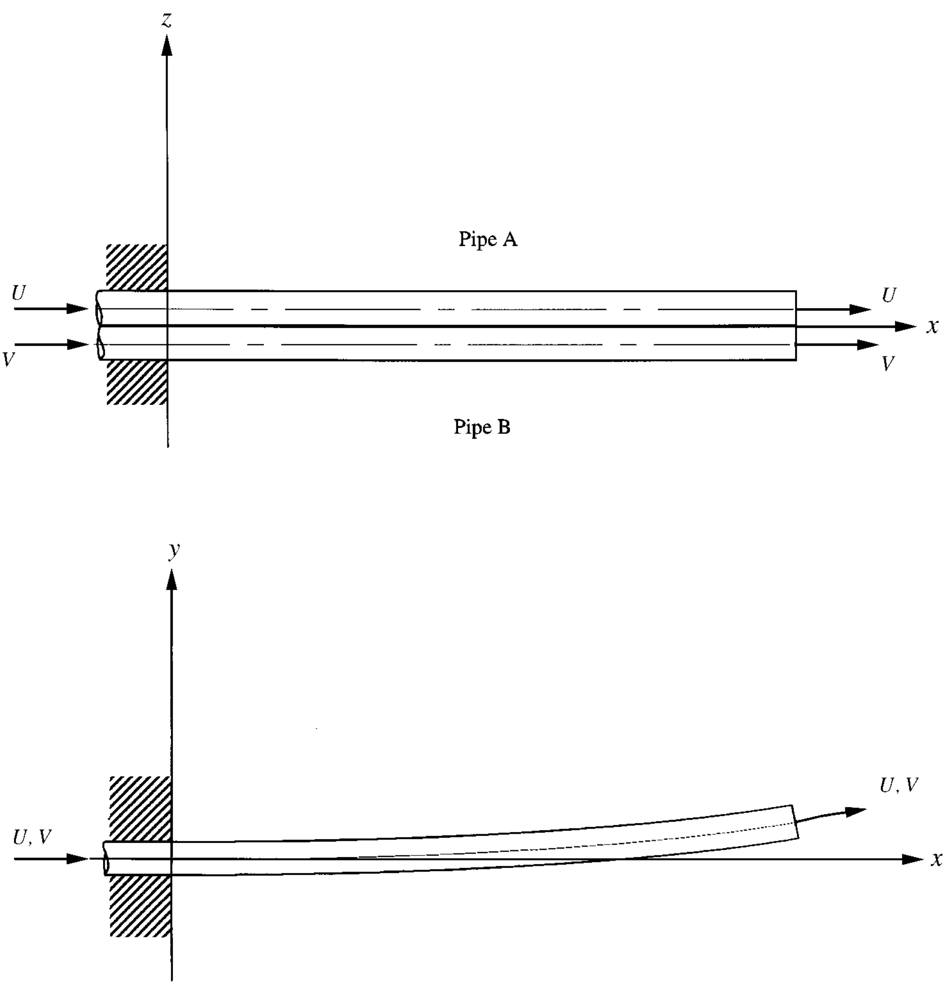

Figure 1. The cantilevered two-pipe system.

Ignoring shear deflection and rotatory inertia, the energy and work terms are:

(i) kinetic energy of the empty pipes

$$T_{\text{pipes}} = \frac{1}{2}(m_A + m_B)\int_0^L \left(\frac{\partial y}{\partial t}\right)^2 \mathrm{d}x, \tag{3}$$

(ii) kinetic energy of the enclosed fluid

$$T_{\text{fluid}} = \frac{1}{2}(M_A + M_B)\int_0^L \left(\frac{\partial y}{\partial t}\right)^2 \mathrm{d}x, \tag{4}$$

(iii) elastic energy of the pipes

$$V_{\text{pipes}} = \frac{1}{2}(EI_A + EI_B)\int_0^L \left(\frac{\partial^2 y}{\partial x^2}\right)^2 \mathrm{d}x, \tag{5}$$

(iv) work done on the structure by the conservative part of the fluid forces

$$W_C = \frac{1}{2}\left(M_A U^2 + M_B V^2\right)\int_0^L \left(\frac{\partial y}{\partial x}\right)^2 \mathrm{d}x, \tag{6}$$

(v) virtual work done on the structure by nonconservative part of the fluid forces

$$\delta W_N = -\Bigg[\underbrace{(M_A U + M_B V)\frac{\partial y}{\partial t}}_{\text{Coriolis force}} + \underbrace{(M_A U^2 + M_B V^2)\frac{\partial y}{\partial x}}_{\text{Fluid jet reaction force}}\Bigg]_{x=L} \delta y(L,t). \tag{7}$$

In a cantilevered fluid-conveying pipe the Coriolis force always acts as a damping mechanism which will be referred to as *fluid damping* [see Chen (1981, 1987), and Section 5.1]. The reaction force due to the momentum flux out of the free end, $M_A U^2 + M_B V^2$, acts as a "*follower*" *load*, as in Beck's column.

By introducing the dimensionless quantities

$$\xi = \frac{x}{L}, \quad \eta = \frac{y}{L}, \quad \tau = \frac{t}{L^2}\sqrt{\frac{EI_A}{m_A + M_A}}, \quad u = UL\sqrt{\frac{M_A}{EI_A}}, \quad v = VL\sqrt{\frac{M_B}{EI_A}},$$
$$\beta_A = \frac{M_A}{m_A + M_A}, \quad \beta_B = \frac{M_B}{m_A + M_A}, \quad \mu = \frac{m_B + M_B}{m_A + M_A}, \quad \sigma = \frac{EI_B}{EI_A}, \tag{8}$$

the energy terms can be written in dimensionless form, as

$$T_{\text{pipes}} = \frac{1}{2}(1 + \mu - \beta_A - \beta_B)\int_0^1 \left(\frac{\partial \eta}{\partial \tau}\right)^2 \mathrm{d}\xi, \qquad T_{\text{fluid}} = \frac{1}{2}(\beta_A + \beta_B)\int_0^1 \left(\frac{\partial \eta}{\partial \tau}\right)^2 \mathrm{d}\xi, \tag{9, 10}$$

$$V_{\text{pipes}} = \frac{1}{2}(1 + \sigma)\int_0^1 \left(\frac{\partial^2 \eta}{\partial \xi^2}\right)^2 \mathrm{d}\xi, \qquad W_C = \frac{1}{2}(u^2 + v^2)\int_0^1 \left(\frac{\partial \eta}{\partial \xi}\right)^2 \mathrm{d}\xi, \tag{11, 12}$$

$$\delta W_N = -\left[(u\sqrt{\beta_A} + v\sqrt{\beta_B})\frac{\partial \eta}{\partial \tau} + (u^2 + v^2)\frac{\partial \eta}{\partial \xi}\right]_{\xi=1} \delta\eta(1,\tau). \tag{13}$$

In order to determine the stability of the oscillations, the pipe-system is divided into a number of finite elements. Within each element, the lateral deflection is represented in complex form as

$$(\eta_c)_e = \mathbf{N}\mathbf{d}_e, \tag{14}$$

where $\mathbf{N}$ is a real row vector of shape functions [Hermitian polynomials, e.g. Cook *et al.* (1989)] and $\mathbf{d}_e$ is a complex column vector representing nodal displacements and rotation in one element. It is noted that the physical deflection is given by $\eta(\xi, \tau) = \mathscr{Re}\{\eta_c(\xi, \tau)\}$. By inserting the energy expressions and equation (14) into equation (1) and carrying out the variations, the equation of motion is obtained in the finite element form

$$\mathbf{M}\ddot{\mathbf{d}} + \mathbf{C}(u, v)\dot{\mathbf{d}} + [\mathbf{S} - \mathbf{Q}(u, v)]\,\mathbf{d} = \mathbf{0}, \tag{15}$$

where $(\dot{\ }) = \partial(\ )/\partial\tau$. The boundary conditions used and implemented in equation (15) are

$$\eta(0, \tau) = \eta'(0, \tau) = 0 \quad \text{and} \quad \eta''(1, \tau) = \eta'''(1, \tau) = 0, \tag{16}$$

where $(\ )' = \partial(\ )/\partial\xi$. With the column divided into N_e finite elements, the matrix system (15) is of size $2N_e \times 2N_e$. The mass matrix $\mathbf{M}$ and the stiffness matrix $\mathbf{S}$ are symmetric, while the Coriolis matrix $\mathbf{C}$ and the load matrix $\mathbf{Q}$ are nonsymmetric.

By assuming an exponential time dependence in the form

$$\mathbf{d}(\xi, \tau) = \mathbf{d}(\xi)\exp(\lambda\tau), \qquad \lambda = \mathscr{Re}\lambda \pm \mathrm{i}\mathscr{Im}\,\lambda = \alpha \pm \mathrm{i}\omega, \quad \mathrm{i} = \sqrt{-1}, \tag{17}$$

an eigenvalue problem in λ is obtained. In order to determine these eigenvalues, equation (15) [with equation (17) inserted] is rewritten as

$$\begin{bmatrix} \mathbf{Q} - \mathbf{S} & \mathbf{0} \\ \mathbf{0} & \mathbf{M} \end{bmatrix} \begin{Bmatrix} \mathbf{d} \\ \lambda\,\mathbf{d} \end{Bmatrix} = \lambda \begin{bmatrix} \mathbf{C} & \mathbf{M} \\ \mathbf{M} & \mathbf{0} \end{bmatrix} \begin{Bmatrix} \mathbf{d} \\ \lambda\,\mathbf{d} \end{Bmatrix}. \tag{18}$$

The QR-algorithm [e.g., Press *et al.* (1992)] is now applied to equation (18). To plot stability diagrams, pairs of the smallest values of u and v which correspond to $\alpha = 0$ (the stability/instability boundary) in equation (17) must be found. This is done by using the bisection method. For calculation of the stability diagrams, the number of finite elements were ten, $N_e = 10$. For the plots of flutter vibrations, 20 finite elements were used.

3. TORSIONAL INSTABILITY

The axial flow through the pipes may also cause torsional instability. The work of Hermann & Nemat-Nasser (1967) can be applied to two-pipe systems having a cross-section with two axes of symmetry. As the cross-section is closed, warping cannot occur and thus, torsional flutter cannot occur. The differential equation for torsional buckling is

$$\{r^2(M_A U^2 + M_B V^2) - GJ\}\,\frac{\mathrm{d}^2\varphi}{\mathrm{d}x^2} = 0, \tag{19}$$

where φ is the torsion angle, r is the polar radius of gyration and GJ the total torsional stiffness of the cross-section. The boundary conditions for the cantilever are: $\varphi(0) = \mathrm{d}\varphi(L)/\mathrm{d}x = 0$. Torsional buckling occurs when

$$M_A U^2 + M_B V^2 = GJ/r^2$$

TABLE 1

Geometrical data and calculated values of the critical flow speeds for transverse flutter and torsional buckling for three different silicone rubber two-pipe systems conveying water

Test pipe	A	B	C
L [m]	0·530	0·530	0·505
D [m]	0·01302	0·00931	0·0122
d [m]	0·00683	0·00684	0·01002
β	0·249	0·505	0·780
w_{fl}	6·20	9·36	13·35
w_{tor}	83·25	105·95	73·88

or, in terms of the dimensionless flow speeds defined in equation (8),

$$u^2 + v^2 = \frac{GJ}{EI_A}\frac{L^2}{r^2} = \frac{16}{1+\nu}\frac{L^2}{D^2+d^2}, \tag{20}$$

where D and d are the external and internal pipe diameter, respectively, and ν is Poisson's ratio.

To get some idea of whether or not torsional buckling is likely to occur before the onset of transverse flutter, two identical silicone rubber pipes conveying water at identical flow speeds $u = v = w$ are considered. The data for three different pipes (test pipe A, B and C, not to be confused with the notation "pipe A" and "pipe B" used elsewhere in this paper) from Sugiyama *et al.* (1984) are used and Poisson's ratio is assumed to be 0·5. The results are summarized in Table 1. It will be seen that the torsional buckling speeds w_{tor} are much higher than the transverse flutter speeds w_{fl}.

As pointed out by Nemat–Nasser & Hermann (1966), cross-section with just one axis of symmetry may lead to coupled torsional–transverse bending oscillations. In light of Table 1, however, the development of a theory accounting for such coupled oscillations has not been pursued in this study and in the remainder of the paper, only plane transverse oscillations will be considered.

4. NUMERICAL RESULTS

4.1. SAME MASS RATIOS

Figure 2 shows the stability diagram for cases where the two pipes and the fluid therein are identical. This means that the fluid mass ratios $\beta_A = \beta_B = \beta$, the total mass ratio $\mu = 1$ and the stiffness ratio $\sigma = 1$.

For $\beta = 0_+$ (a very small positive value; 10^{-9} in the numerical calculations), the fluid damping is insignificant and the stability curve is just the circle section $(u^2 + v^2)/2 \approx (4{\cdot}19)^2$. The value 4·19 is in agreement with the critical flow speed for a pipe with a small but non-zero β found by Gregory & Païdoussis (1966). For larger values of β there are regions where the slope of the stability curve, $\mathrm{d}u/\mathrm{d}v$, is positive. Physically this means that one fluid extracts energy from the other and thus stabilizes the system. For $\beta = 0{\cdot}50$, 0·75 and 0·90 there is an interval of $v(u)$ where, *after* loss of stability, further increase in $u(v)$ implies that stability is regained and then lost again by continued increase of $u(v)$. Such stability curve inflections are characteristic for the cantilevered fluid-conveying pipe. They are also seen, for example, in stability diagrams depicting the critical flow speed as a function of the mass

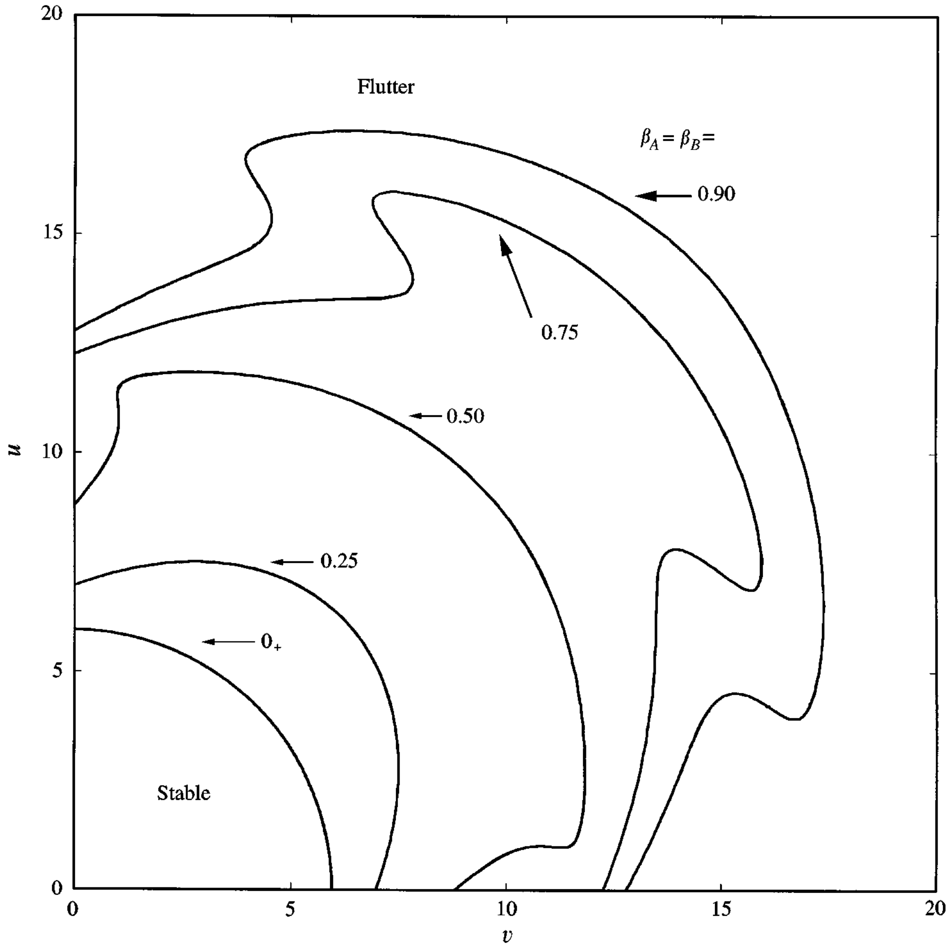

Figure 2. Stability diagram for two identical pipes conveying identical fluids at different flow speeds u and v.

ratio β (Gregory & Païdoussis 1966) and as a function of a gravity parameter (Bishop & Fawzy 1976). An explanation is provided by Figure 3 which is for $\beta = 0{\cdot}75$. The leading eigenvalues, i.e., those eigenvalues having the largest real parts, are depicted as functions of the flow speed u in pipe A. The flow speed in pipe B is constant, $v = 7{\cdot}50$. Only the upper half-plane is shown, but as the matrices in equation (15) are real, all branches have a mirror-image in the lower half-plane. The branch labeled I becomes unstable for $u = 13{\cdot}60$, is restabilized by $u = 14{\cdot}71$, and then again becomes unstable for $u = 15{\cdot}96$. There is another way in which inflections on the stability curve can occur, namely if branch I remained stable for $u > 14{\cdot}71$ but another branch, II or III say, entered the right half-plane at $u \approx 16$.

4.2. Different Mass Ratios

Figure 4 shows the stability diagram for cases where the fluid mass ratio β_B in pipe B is varied while the fluid mass ratio in pipe A is held constant ($\beta_A = 0{\cdot}25$). In order to compare with Figure 2, the total mass ratio $\mu = 1$ and the stiffness ratio $\sigma = 1$. The figure shows that

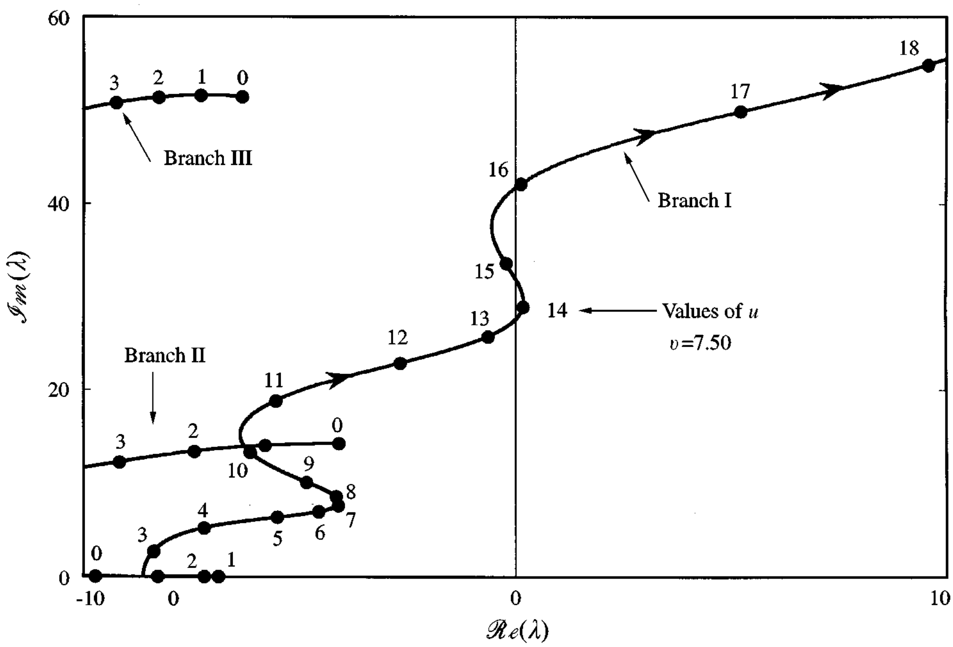

Figure 3. Root-locus diagram for $\beta_A = \beta_B = 0{\cdot}75$. The flow speed u in pipe A is varied, while that in pipe B is constant and equal to $v = 7{\cdot}50$.

if the purpose of the flow in pipe B is to stabilize the system, such that the flow speed in pipe A can be as large as possible, then β_B should be as large as possible. When $\beta_B = 0_+$, increasing v implies an increase of the total "follower" end load without significant increase of the total fluid damping. Therefore, to remain at the stability boundary, u must be decreased.

The purpose of the root-locus diagrams shown in Figure 5 is to more directly explain the stabilizing effect one fluid may have on the other. The diagrams are related to the stability curve for $\beta_B = 0{\cdot}50$ in Figure 4. In Figure 5(a), the fluid in pipe B is still, $v = 0$. Then all roots are located on the imaginary axis for $u = 0$. Stability is lost at $u = 6{\cdot}97$ where branch II enters the right half-plane. In Figure 5(b) the fluid in pipe B has the speed $v = 5{\cdot}46$, corresponding to the "top" in the stability curve depicted in Figure 4. It is thus the most stabilizing speed. In the root-locus diagram, the effect is that all branches $\lambda(u)$ are shifted to the left. Stability is now lost at $u = 10{\cdot}32$, also in branch II. The steep top on the stability curve appears when the "kink" on branch II (present from $u = 9$ to 10) is moved into the left half-plane.

Figure 6 shows the stability diagram for cases where the fluid in pipe A is very "light" ($\beta_A = 0_+$). It will be seen that a very "heavy" fluid (large value of β_B) in pipe B and a very large value of its flow speed v is required to increase the critical value of u. Moderate Coriolis forces have a destabilizing effect.

Returning briefly to the discussion of torsional buckling in Section 3, by using equation (20) and assuming that $\beta_A = \beta_B = 0{\cdot}9$ is the upper bound of practically realisable β-values, the following result is obtained. For any $\beta_A, \beta_B \in (0, 0{\cdot}9)$, torsional buckling will not occur at lower flow speed than transverse flutter if

$$\frac{1}{1+\nu}\frac{L^2}{D^2+d^2} > \frac{1}{8}(14{\cdot}33)^2 \approx 25{\cdot}67. \tag{21}$$

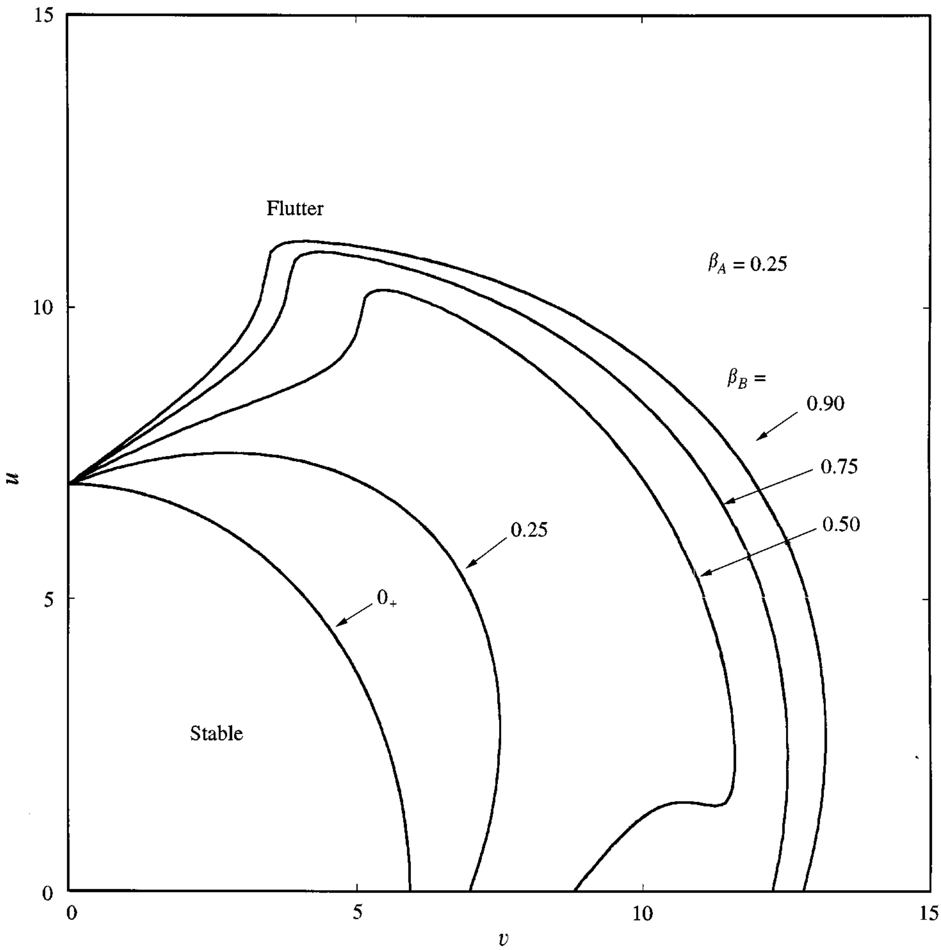

Figure 4. Stability diagram for different values of fluid mass ratio β_B, with $\beta_A = 0{\cdot}25$. The total mass ratio $\mu = 1$ and the stiffness ratio $\sigma = 1$.

4.3. Simultaneous "Forward and "Reverse" Flow

The case of two identical pipes conveying identical fluids is reconsidered but now the flow in pipe A is reversed (flow speed $u < 0$). [The same equation of motion (15) and the same boundary conditions (16) are used.] The stability curves are shown in Figure 7. As shown by Païdoussis & Luu (1985), an aspirating pipe loses, at least in theory, stability by flutter at an arbitrarily small but non-zero flow speed because of negative fluid damping. (Including structural damping, or damping from the surrounding fluid, increases the critical flow speed). As will be seen from Figure 7, the effect of increasing the flow speed in pipe B from $v = 0$ to values > 0 is cancellation of the fluid damping. The total fluid loading is thus reduced to a pure follower load, as by Beck's column.

For any non-zero mass ratio $\beta = \beta_A = \beta_B$, the stability curves are straight lines until the flow speeds reach the values $(u, v) = (-\,4{\cdot}19,\ 4{\cdot}19)$. [In theory, if the fluid damping is perfectly cancelled, the straight line continues to $(u, v) = \{-\sqrt{(20{\cdot}05)},\ \sqrt{(20{\cdot}05)}\} = (-\,4{\cdot}48,\ 4{\cdot}48)$. The numerical value of 20·05 corresponds to the dimensionless critical load $P_{\text{crit}}L^2/(EI)$ of Becks column, e.g., Leipholz (1980).] By increasing the flow speed in pipe

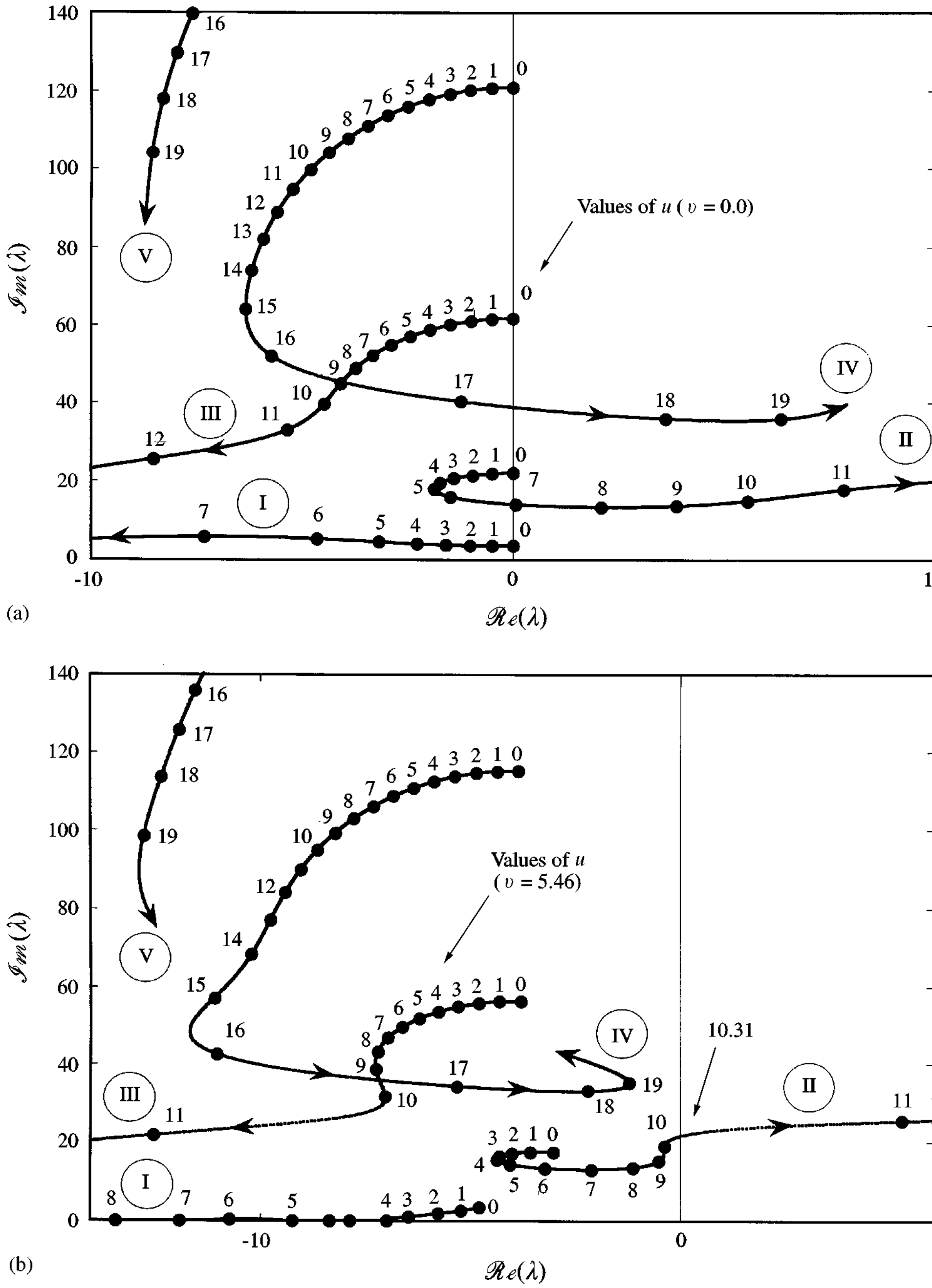

Figure 5. Root-locus diagram for $\beta_A = 0{\cdot}25$, $\beta_B = 0{\cdot}50$, $\mu = 1$ and $\sigma = 1$. (a) Flow speed u is varied while flow speed $v = 0{\cdot}0$. (b) u is varied while $v = 5{\cdot}46$.

B beyond the value 4·.19, the critical flow rate in pipe A is gradually reduced for all β-values. However, the stability curves for $\beta = 0{\cdot}75$ and $0{\cdot}90$ also have inflections for $u < 0$.

It has been shown that attaching a pipe with "forward" flow to an otherwise identical aspirating pipe constitutes a very efficient stabilization aid. As already mentioned in

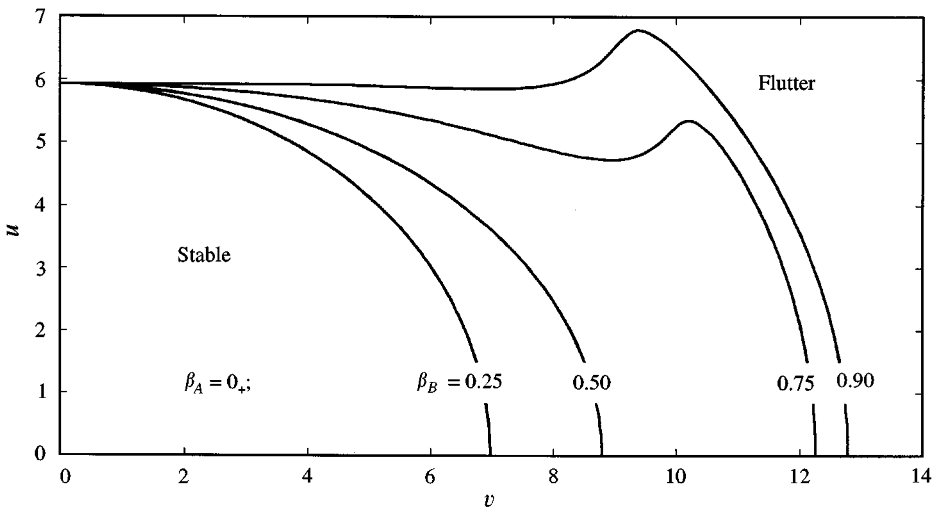

Figure 6. Stability diagram for cases with a very light fluid in pipe A ($\beta_A = 0_+$, $\mu = 1$, $\sigma = 1$).

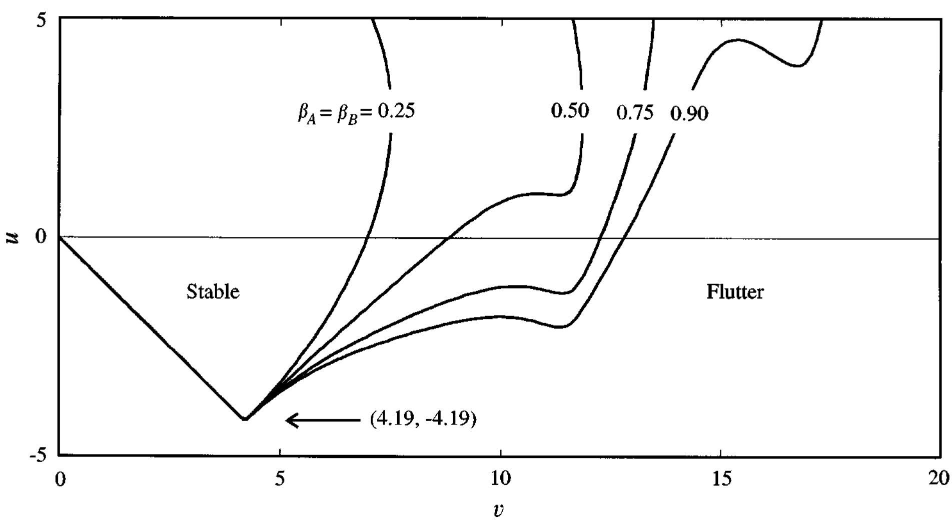

Figure 7. Stability diagram for "reverse" flow in pipe A ($u < 0$) and "forward" flow in pipe B ($v > 0$) ($\beta_A = \beta_B$, $\mu = 1$, $\sigma = 1$).

Section 1, however, application of the boundary conditions (16) to the aspirating pipe may be questioned as the flow into the pipe may not be purely tangential. Flutter instability of the aspirating pipe has not yet been verified by experiment. In whatever way, attaching a pipe with a moderate "forward" flow to an aspirating pipe is an efficient means of reducing the time of transient vibrational response to disturbances, cf. Sugiyama *et al.* (1996).

5. SOME ENERGY AND BENDING WAVE CONSIDERATIONS

5.1. Basic Equations

Benjamin (1961) showed that, during a time interval $[\tau_1, \tau_2]$ where the shape of the pipes is the same at τ_2 as at τ_1, the energy delivered to the tubes by the fluid is given by

$$\Delta W_N = -\int_{\tau_1}^{\tau_2} \frac{\partial \eta}{\partial \tau}\left[(u\sqrt{\beta_A} + v\sqrt{\beta_B})\frac{\partial \eta}{\partial \tau} + (u^2+v^2)\frac{\partial \eta}{\partial \xi}\right]_{\xi=1} \mathrm{d}\tau. \tag{22}$$

The first term is associated with the Coriolis force. As this term is always negative (for $u, v > 0$) the Coriolis force acts as a damping mechanism. At the stability threshold (flutter boundary) the vibrations are of constant amplitude, and over one period, $\Delta W_N = 0$. The pipe deflection can be written in the form

$$\eta(\xi,\tau) = \mathscr{Re}\{\eta_e(\xi,\tau)\} = A(\xi)\exp(\alpha\tau)\cos(\omega\tau + \theta(\xi)). \tag{23}$$

Here $A(\xi)$ is the amplitude and $\theta(\xi)$ is the phase angle. Inserting equation (23) into equation (22), with $\alpha = 0$, $\tau_1 = 0$, $\tau_2 = 2\pi/\omega$ and $\Delta W_N = 0$, gives the phase speed of the travelling bending wave at the free end, $\xi = 1$, as

$$c_1 = \frac{\omega}{k_1} = \frac{\omega}{-(\partial\theta/\partial\xi)_{\xi=1}} = \frac{u^2+v^2}{\sqrt{\beta_A}u + \sqrt{\beta_B}v}. \tag{24}$$

Here k_1 is the wavenumber at the free end. Equation (24) is, of course, only valid for $\sqrt{(\beta_A)}u + \sqrt{(\beta_B)}v \neq 0$. When the denominator is zero there is no Coriolis force and thus no travelling wave. In physical variables, equation (24) takes the form

$$c_L = \frac{M_A U^2 + M_B V^2}{M_A U + M_B V} = \frac{\text{total momentum flux}}{\text{total mass flow rate}}. \tag{25}$$

For a single pipe ($v = 0$, $\beta_B = 0$), equation (24) reduces to

$$c_1 = \frac{u}{\sqrt{\beta_A}}; \tag{26}$$

see also Langthjem (1996) and Lee & Mote (1997). In physical variables, equation (26) takes the simple form

$$c_L = U. \tag{27}$$

The free jet present at $x > L$ also performs steady-state oscillations at the flutter-limit and the wave speed in the pipe at $x = L$ must match the wave speed of a neutral disturbance of the jet for $x \geq L$. This is the case, since equation (27) is identical to the result for a free "plug-flow" jet obtained by Batchelor & Gill (1962).

5.2. Simplified Calculations of the Critical Flow Speed Values from the Phase Speed–Flow Speed Relation

For a single pipe with a given mass ratio β_A, relations (24) and (26) show that the dimensionless critical flow speed is directly proportional to the flutter frequency and inversely proportional to the wavenumber at the free end. For the two-pipe system the nonlinear connection between the two flow speeds makes the relation less clear. Table 2 gives, for $\beta_A = \beta_B$, values of flow speeds u and v, flutter frequency ω, tip-end wavenumber k_1 and tip-end phase speed c_1 at the flutter limit for two cases: (i) when $u = v$ and (ii) when v has the most stabilizing value such that the maximum value of u is obtained. It will be seen that c_1 is only slightly larger for configuration (ii) than for configuration (i) in all cases.

TABLE 2

Case of *indentical* mass ratios β_A and β_B ($\mu = 1$, $\sigma = 1$). Values of flow speeds u and v, flutter frequency ω, tip-end wavenumber k_1 and tip-end phase speed c_1 at the flutter limit. When $v \neq u$, v has the most stabilizing value which gives the largest value of u

$\beta_A = \beta_B$	u	v	ω	k_1	c_1
0·25	6·21	6·21	13·61	1·10	12·43
0·25	7·51	2·73	13·69	1·10	12·47
0·50	9·32	9·32	26·50	2·01	13·18
0·50	11·84	2·70	25·31	1·76	14·34
0·75	13·14	13·14	44·54	2·94	15·17
0·75	15·94	7·48	41·64	2·72	15·29
0·90	14·33	14·33	45·63	3·02	15·11
0·90	17·36	6·53	44·51	2·93	15·18

TABLE 3

Case of *different* mass ratios β_A and β_B ($\beta_A = 0{\cdot}25$, $\mu = 1$, $\sigma = 1$). Values of u, v, ω, k_1 and c_1 at the flutter limit. $\partial u/\partial v = 0$ at the points (u, v) for which $u > v$; $\partial v/\partial u = 0$ at the points (u, v) for which $v > u$

β_B	u	v	ω	k_1	c_1
0·50	10·31	5·46	21·64	1·43	15·10
0·50	2·25	11·61	23·17	1·55	14·98
0·75	10·96	4·35	22·82	1·52	15·03
0·75	2·35	12·52	26·42	1·96	13·50
0·90	11·14	4·13	23·70	1·59	14·88
0·90	2·72	13·18	26·45	2·03	13·06

Table 3 gives similar values for cases where $\beta_A \neq \beta_B$ ($\beta_A = 0{\cdot}25$). Also here, the changes in c_1 for given β_A and β_B are not large. If one point on the stability curve is known, a reasonably accurate estimate on how a change in one flow speed affects the other can be obtained from equation (24) with c_1 assumed to be a constant. Equation (24) can then be rewritten in the form

$$\left(u - \frac{1}{2}c_1\sqrt{\beta_A}\right)^2 + \left(v - \frac{1}{2}c_1\sqrt{\beta_B}\right)^2 = \left(\frac{1}{2}c_1\sqrt{\beta_A + \beta_B}\right)^2. \tag{28}$$

This is simply a circle with radius $= 1/2c_1\sqrt{\beta_A + \beta_B}$ and centre in $1/2c_1(\sqrt{\beta_A}, \sqrt{\beta_B})$. Figures 2 and 4 show that most parts of the stability curves are indeed circle sections. This reflects that the effects of the two individual flows, with good approximation, are directly additive here. The estimate from equation (28) is of course not useful across any inflection on a stability curve. Equation (28) is particularly useful for estimating the critical flow-speed pair for two identical pipes conveying identical fluids at different flow speeds from the knowledge about the critical flow speed for a single pipe. For example, if the flow speed v in pipe B is set as 0·6 times the critical flow speed for a single pipe, what is the new critical value of the flow speed u in pipe A? Table 4 shows such estimates, compared with results from finite element calculations. The values for $\beta = 0{\cdot}25$, 0·75and 0·90 agree to within 1%. The values for $\beta = 0{\cdot}5$ agree to within 2·5%. It is emphasized, however, that equation (28) can

TABLE 4

Comparison of approximate "two-pipe" critical flow speed values $(u_{tp}, v_{tp}) = (u_{tp}, 0{\cdot}6u_{sp})$, estimated from the known critical flow speed u_{sp} for a single pipe by use of equation (28), with "true" values (from finite element calculations)

$\beta_A = \beta_B$	u_{sp}	c_1 by eq. (24)	u_{tp} for $v_{tp} = 0.6u_{sp}$ by equation (26)	u_{tp} for $v_{tp} = 0.6u_{sp}$ by FEM
0·25	6·21	12·43	7·46	7·43
0·50	9·32	13·18	11·18	11·46
0·75	13·14	15·17	15·76	15·90
0·90	14·33	15·11	17·20	17·16

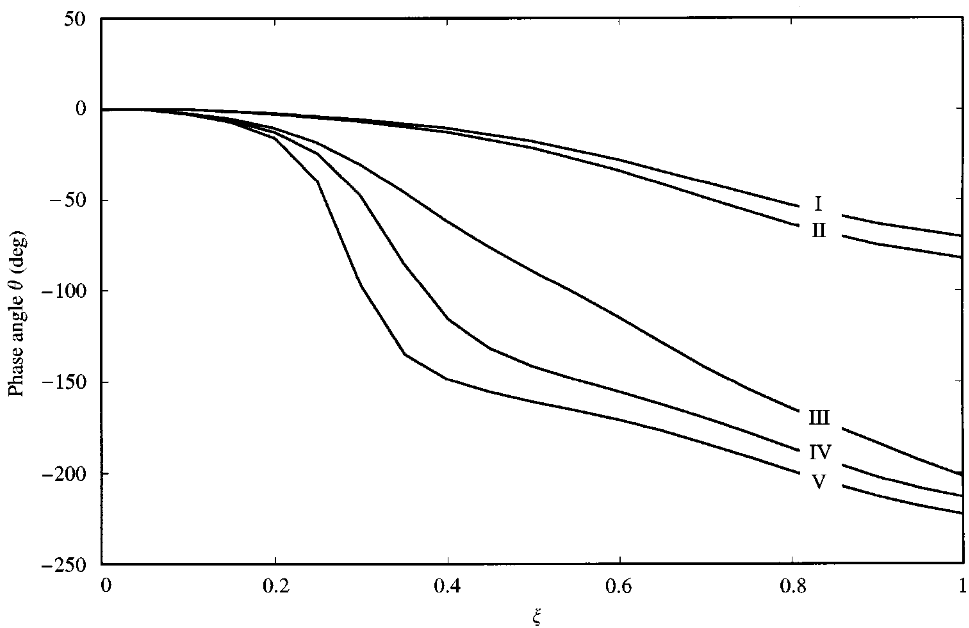

Figure 8. Phase-angle distributions for five flutter cases. I: $\beta_A = \beta_B = 0{\cdot}25$, $u = v = 6{\cdot}21$; II: $\beta_A = \beta_B = 0{\cdot}25$, $u = 7{\cdot}51$, $v = 2{\cdot}73$; III: $\beta_A = \beta_B = 0{\cdot}90$, $u = v = 14{\cdot}33$; IV: $\beta_A = 0{\cdot}25$, $\beta_B = 0{\cdot}90$, $u = 11{\cdot}14$, $v = 4{\cdot}13$; V: $\beta_A = 0{\cdot}25$, $\beta_B = 0{\cdot}50$, $u = 10{\cdot}31$, $v = 5{\cdot}46$.

only give a useful "first estimate", as jumps and inflections on the stability curves may occur, as seen in Figures 2 and 4.

6. FLUTTER OSCILLATIONS

Figure 8 shows the phase-angle distributions $\theta(\xi)$ for five flutter cases which are points on the stability curves in Figures 2 and 4. The curves labelled I and III are for two identical fluids ($\beta_A = \beta_B = 0{\cdot}25$ and $0{\cdot}90$, respectively) flowing with identical speeds at the flutter limit ($u = v = 6{\cdot}21$ and $14{\cdot}33$, respectively). These systems are thus equivalent to single pipes. That the phase-angle θ decreases for increasing ξ explains the well-known "dragging" nature of the oscillations. Except for a small part near the clamped end, θ is approximately a linear function of ξ. Thus, the wavenumber function $k(\xi) \simeq k_1$, the wavenumber at the free

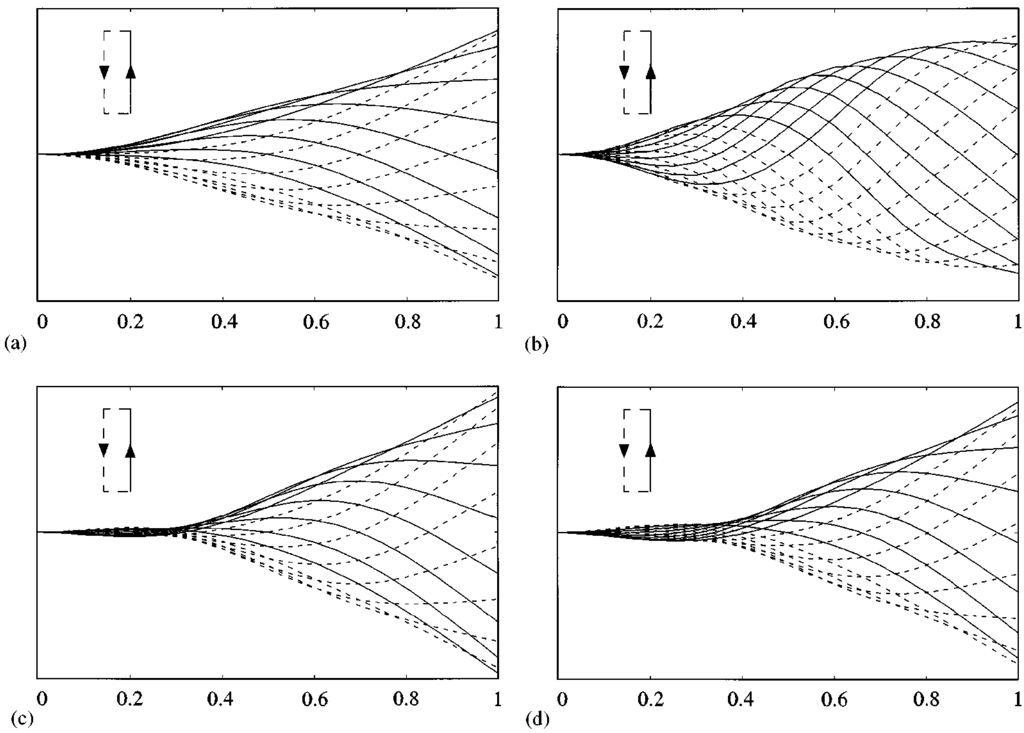

Figure 9. Flutter oscillations. The diagrams refer to the direction of motion of the free end. (a) $\beta_A = \beta_B = 0{\cdot}25$, $u = v = 6{\cdot}21$; (b) $\beta_A = \beta_B = 0{\cdot}90$, $u = v = 14{\cdot}33$; (c) $\beta_A = 0{\cdot}25$, $\beta_B = 0{\cdot}50$, $u = 10{\cdot}31$, $v = 5{\cdot}46$; (d) $\beta_A = 0{\cdot}25$, $\beta_B = 0{\cdot}90$, $u = 11{\cdot}14$, $v = 4{\cdot}13$.

end. This means that the bending wave travelling along the tube travels approximately with the flow speed U (in dimensionless variables, with the speed $u/\sqrt{\beta}$). This is manifested in the well-known "smooth" flutter-oscillations, as depicted in Figures 9(a, b). Solid lines correspond to upward motions of the free end; dashed lines to downward motions. The time step between the lines is $\Delta\tau = \pi/(8\omega)$.

Curve II is also for two identical fluids ($\beta_1 = \beta_2 = 0{\cdot}25$) but now the fluid in pipe B flows at $v = 2{\cdot}73$, the most stabilizing value. The flow speed in pipe A is $u = 7{\cdot}51$. The phase speed of the travelling bending wave will be slightly more varying than that associated with Curve I. Curve V corresponds the root-locus diagram shown in Figure 5(b), that is $\beta_A = 0.25$, $\beta_B = 0{\cdot}50$, $u = 10{\cdot}31$ and $v = 5{\cdot}46$. Here there is a steep drop in the phase-angle for $0{\cdot}2 < \xi < 0{\cdot}4$. For $\xi > 0{\cdot}5$, $k(\xi) \simeq k_1$, as for curves I and II. The flutter oscillations are shown in Figure 9(c). It is remarkable that the amplitude is very small for a part near the clamped end. The situation is similar in Figure 9(d) which shows the flutter oscillations of a pipe with $\beta_A = 0{\cdot}25$, $\beta_B = 0{\cdot}90$, $u = 11{\cdot}14$ and $v = 4{\cdot}13$ (the most stabilizing speed). The corresponding phase-angle is included in Figure 8 as Curve IV.

The amplitude reduction near the clamped end can be understood by imaging the flutter oscillations expanded in eigenmodes (eigenfunctions), as by Galerkin's method. As the value of β (for a single pipe) is increased, higher and higher modes become significant. This can be seen by comparing Figures 9(a) and 9(b). Superposition of the oscillation initiated by the flow through pipe B alone with those initiated by the flow through pipe A alone gives a "destructive interference" near the clamped end. This can be seen by imaging a direct superposition of Figures 9(a) and 9(b).

In terms of equation (22) flutter occurs when $\Delta W > 0$, meaning that during one period of oscillation, the fluid jet has delivered more energy to the system (solid + enclosed fluid) than can be dissipated by the fluid damping mechanism. As explained by Benjamin (1961), this can only occur if $(\partial\eta/\partial\tau)_{\xi=1}$ and $(\partial\eta/\partial\xi)_{\xi=1}$ are sufficiently out of phase such that $(\partial\eta/\partial\tau \times \partial\eta/\partial\xi)_{\xi=1} < 0$ during most part of the time interval $[\tau_1, \tau_2]$. This "sloping backwards" of the tip end is likely reduced when the length of the vibrating part is decreased. This provides a possible physical explanation of the stabilizing effect of the flow in pipe B.

The ratios (u_{cr} for $v = 0$)/(u_{cr} for $v =$ "the most stabilizing value") appear to be close to the lengths of the "fully" vibrating pipe parts. For Figure 9(c), the ratio is 6·97/10·31 ≈ 0.68 and for Figure 9(d), 6·97/11·14 ≈ 0·63. [It is noticed that the (physical) critical flow speed U_{cr} in a single pipe is increased proportionally to the reduction of the length L; see the definition of the dimensionless flow speed u in equation (8)].

7. CONCLUSION

Dynamic stability of a cantilevered two-pipe system conveying different fluids has been investigated. Various aspects concerning the energy balance between the solid and the two "competing" axial fluid flows have been discussed. The main conclusions are the following.

(1) One fluid flow may dissipate energy delivered to the system by the other flow, thus acting as a stabilizer. The stabilizing effect is largest when the mass ratio of the stabilizing flow is large. In some cases, however, addition of fluid damping may have a destabilizing effect, especially when the mass ratio of one fluid is very small.

(2) In the case of two identical pipes conveying identical fluids, when one pipe has "forward" flow and the other pipe "reverse" flow, the fluid damping cancels out and the total fluid loading is reduced to a pure "follower" load. The system is thus, in principle, reduced to Beck's column.

(3) At the flutter limit, the phase speed of the travelling bending wave at the free end of the two-pipe system equals (total momentum flux)/(total mass flow rate). Phase angle plots show that the phase speed is approximately constant along the downstream half of the pipes.

(4) The phase speed [the ratio (total momentum flux)/(total mass flow rate)] at the free end varies only slightly along parts of the flutter boundaries (stability curves). This gives a very simple approximate relation between the two flow speeds there.

ACKNOWLEDGEMENTS

Financial support for this investigation is due to the Japan Society for the Promotion of Science (JSPS). The first author (ML) would like to express his deep gratitude to JSPS for a Post-doctoral Fellowship (fiscal years 1996 and 1997) to conduct research in Japan. The support from the Danish Research Academy and from Prof. Pauli Pedersen at the Technical University of Denmark is also gratefully acknowledged.

REFERENCES

Batchelor, G.K. & Gill, A.E. 1962 Analysis of the stability of axisymmetric jets. *Journal of Fluid Mechanics* **14,** 529–551.

Benjamin, T.B. 1961 Dynamics of a system of articulated pipes conveying fluid. I. Theory. *Proceedings of the Royal Society* (*London*) A **261,** 457–486.

Bishop, R.E.D. & Fawzy, I. 1976 Free and forced oscillations of a vertical tube containing a flowing fluid. *Philosophical Transactions of the Royal Society* (*London*) **284,** 1–47.

Bolotin, V.V. 1963 *Nonconservative Problems of the Theory of Elastic Stability*. Oxford: Pergamon Press.

Chen, S.-S. 1981 Fluid damping for circular cylindrical structures. *Nuclear Engineering and Design* **63,** 81–100.

Chen, S.-S. 1987 *Flow-Induced Vibration of Circular Cylindrical Structures*. Washington: Hemisphere Publishing Corporation.

Cook, R.D., Malkus, D.S. & Plesha, M.E. 1989 *Concepts and Applications of Finite Element Analysis*. New York: Wiley.

Dowell, E.H., Curtiss, H.C. Jr., Scanlan, R.H. & Sisto, F. 1989 *A Modern Course in Aeroelasticity*. Dortrecht: Kluwer Academic Publishers.

Gregory, R.W. & Païdoussis, M.P. 1966 Unstable oscillations of tubular cantilevers conveying fluid. I. Theory. *Proceedings of the Royal Society* (*London*) A **293,** 512–527.

Hannoyer, & Païdoussis, M.P. 1978 Instabilities of tubular beams simultaneously subjected to internal and external axial flows. *ASME Journal of Mechanical Design* **100,** 328–336.

Herrmann, G. & Nemat-Nasser, S. 1967 Instability modes of cantilevered bars induced by fluid flow through attached pipes. *International Journal of Solids and Structures* **3,** 39–52.

Huang, L. 1995 Flutter of cantilevered plates in axial flow. *Journal of Fluids and Structures* **9,** 127–147.

Lamb, H. 1932 *Hydrodynamics*, 6th edition, reprinted 1994. Cambridge: Cambridge University Press.

Langthjem, M.A. 1996 Dynamics, stability and optimal design of structures with fluid interaction. Ph.D. Thesis, DCAMM Report No. S71, Department of Solid Mechanics, Technical University of Denmark, Lyngby, Denmark.

Lee, S.-Y. & Mote, C.D. Jr. 1997 A generalized treatment of the energetics of translating continua, Part II: Beams and fluid conveying pipes. *Journal of Sound and Vibration* **204,** 735–753.

Leipholz, H. 1980 *Stability of Elastic Systems*. Alphen an den Rijn: Sijthoff & Noordhoff.

Nemat–Nasser, & Herrmann, G. 1966 Torsion instability of cantilevered bars subjected to nonconservative loading. *Journal of Applied Mechanics* **33,** 102–104.

Ouchi, K. & Nakahara, H. 1998 An increase of primary production with Deep Ocean Water Upwelling Machine using density current. In *Proceedings of the 14th Ocean Engineering Symposium, The Society of Naval Architects of Japan*. Tokyo, Japan, 16–17 July 1998. pp. 41–48.

Païdoussis, M.P. 1987 Flow-induced instabilities of cylindrical structures. *Applied Mechanics Reviews* **40,** 163–175.

Païdoussis, M.P. 1993 1992 Calvin Rice Lecture: Some curiosity-driven research in fluid structure interactions and its current applications. *ASME Journal of Pressure Vessel Technology* **115,** 2–14.

Païdoussis, M.P. 1997 Fluid–structure interactions between axial flows and slender structures. In *Theoretical and Applied Mechanics 1996* (eds T. Tatsumi, E. Watanabe & T. Kambe), pp. 427–442. Amsterdam: Elsevier Science.

Païdoussis, M.P. & Besançon, P. 1981 Dynamics of arrays of cylinders with internal and external axial flows. *Journal of Sound and Vibration* **76,** 361–380.

Païdoussis, M.P. & Issid, N.T. 1974 Dynamic stability of pipes conveying fluid. *Journal of Sound and Vibration* **33,** 267–294.

Païdoussis, M.P. & Li, G.X. 1993 Pipe conveying fluid: a model dynamical problem. *Journal of Fluids and Structures* **7,** 137–204.

Païdoussis, M.P. Luu, T.P. 1981 Dynamics of a pipe aspirating fluid such as might be used in ocean mining. *ASME Journal of Energy Resources Technology* **107,** 250–255.

Press, W.H., Teukolsky, S.A., Vetterling, W.T. & Flannery, B.P. 1992 *Numerical Recipes in Fortran*. Cambridge: Cambridge University Press.

Sugiyama, Y., Katayama, K., Kanki, E., Nishino, K. & Åkesson, B. 1996 Stabilization of cantilevered flexible structures by means of an internal flowing fluid. *Journal of Fluids and Structures* **10,** 653–661.

Sugiyama, Y., Katayama, K. & Kinoi, S. 1995a Flutter of cantilevered column under rocket thrust. *ASCE Journal of Aerospace Engineering* **8,** 9–16.

Sugiyama, Y., Matsuike, J., Ryu, B.-J., Katayama, K., Kinoi, S. & Enomoto, N. 1995b Effect of concentrated mass on stability of cantilevers under rocket thrust. *AIAA Journal* **33,** 499–503.

Sugiyama, Y., Tanaka, Y., Kishi, T. & Kawagoe, H. 1984 Effect of a spring support on the stability of pipes conveying fluid. *Journal of Sound and Vibration* **100,** 257–270.

Taneda, S. 1968. Waving motions of flags. *Journal of the Physical Society of Japan* **24,** 392–401.

APPENDIX: NOTATION

c_L	phase speed of the travelling bending wave evaluated at the free end
c_1	dimensionless phase speed of the bending wave at the free end
$\mathbf{C}$	Coriolis matrix
$\mathbf{d}$	complex eigenvector
EI_A, EI_B	bending stiffnesses
GJ	torsional stiffness
k_1	wavenumber at the free end
L	total length of the pipe system
m_1, m_2	specific masses of pipes (mass per unit length)
M_A, M_B	specific masses of fluids (mass per unit length)
$\mathbf{M}$	mass matrix
N_e	number of finite elements
$\mathbf{Q}$	fluid load matrix
r	polar radius of gyration
$\mathbf{S}$	stiffness matrix
t	time
T_{pipes}	kinetic energy of empty pipes
T_{fluid}	kinetic energy of enclosed fluid
U, V	fluid speeds
u, v, w	dimensionless fluid speeds
V_{pipes}	potential (elastic) energy
$W, \Delta W$	work
x	distance along tube
y	lateral deflection
α	stability parameter
β_A	the ratio (mass of fluid in pipe A)/(mass of fluid-filled pipe A)
β_B	the ratio (mass of fluid in pipe B)/(mass of fluid-filled pipe B)
η	dimensionless lateral deflection
η_c	dimensionless lateral deflection in complex representation
λ	complex eigenvalue
μ	the ratio (mass of fluid-filled pipe B)/(mass of fluid-filled pipe A)
ξ	dimensionless distance along the tube
σ	the ratio (stiffness of pipe B)/(stiffness of pipe A)
τ	dimensionless time
φ	torsional angle
ω	dimensionless frequency parameter